If the operators $\mathsf{a} = (\alpha|\tau_\alpha)$ of G are expressed in the conventional setting and those of g, say $\mathsf{b} = (\beta|\tau_\beta)$ in a non-conventional setting, belonging to a matrix $\mathbf{S}_j$, one has for the new operators $\mathsf{b}' = (\beta'|\tau'_\beta)$,

$$\mathsf{b} = (\mathbf{S}_j|000)^{-1}\,\mathsf{b}(\mathbf{S}_j|000) = (\mathbf{S}\mathbf{S}_j|\mathbf{T})^{-1}\,\mathsf{a}(\mathbf{S}\mathbf{S}_j|\mathbf{T}). \quad (C2)$$

One may consider more general changes of settings, $\mathsf{S} = (\mathbf{S}_j|\mathbf{T}_j)$, involving a change of axes *and* of origin and use the general formula

$$\mathsf{b}' = (\mathsf{S}\mathsf{S}_j)^{-1}\,\mathsf{a}(\mathsf{S}\mathsf{S}_j). \quad (C3)$$

Example. If $\mathbf{S} = \mathbf{O}_1$ (24) and $\mathbf{S}_j = \mathbf{S}_5$ ($C1$), one has

$$\mathbf{S}\mathbf{S}_j = \begin{bmatrix} 0 & s_{11} & 0 \\ s_{22} & 0 & 0 \\ 0 & 0 & -s_{33} \end{bmatrix}.$$

APPENDIX D
Factorization of matrices

Considering the 2×2 matrix part

$$\begin{bmatrix} s_{11} & -s_{21} \\ s_{21} & s_{11} \end{bmatrix}$$

of determinant $s_{11}^2 + s_{21}^2$, a subgroup is not maximal if the matrix can be factorized into matrices of the same nature (Sayari, 1976). For instance, the factorization scheme for the index $10 = 3^2 + 1^2$ is

$$\begin{bmatrix} 1 & -3 \\ 3 & 1 \end{bmatrix} = \begin{bmatrix} 1 & -1 \\ 1 & 1 \end{bmatrix} \begin{bmatrix} 2 & -1 \\ 1 & 2 \end{bmatrix}, \quad (D1)$$

the intermediate subgroups having the indices $2 = 1^2 + 1^2$ and $5 = 2^2 + 1^2$.

References

BERTAUT, E. F. & BILLIET, Y. (1978). *C.R. Acad. Sci.* **287**, 989–991.

BILLIET, Y. (1973). *Bull. Soc. Fr. Minéral. Cristallogr.* **96**, 327–334.

BILLIET, Y. & LE COZ, M. (1979). *Acta Cryst.* To be submitted.

BUERGER, M. (1947). *J. Chem. Phys.* **15**, 1–16.

International Tables for X-ray Crystallography (1952). Vol. I. Birmingham: Kynoch Press.

KOCH, E. & FISCHER, W. (1978). *Z. Kristallogr.* **147**, 21–38.

SAYARI, A. (1976). Thèse de spécialité, Tunis.

Acta Cryst. (1979). A**35**, 745–756

The Defect Structure of VO_x. I. The Ordered Phase, $VO_{1.30}$

BY M. MORINAGA* AND J. B. COHEN

Department of Materials Science & Engineering, The Technological Institute, Northwestern University, Evanston, IL 60201, *USA*

(*Received* 28 *November* 1978; *accepted* 13 *March* 1979)

Abstract

Integrated X-ray intensities were obtained from a single crystal of $VO_{1.30}$ annealed below the ordering transition. The space group is $I4_1/amd$, and the unit-cell contents are $V_{51.6}O_{64}$. The atomic arrangement is similar to that proposed by Andersson & Gjönnes [*Acta Chem. Scand.* (1970), **24**, 2250–2252], but there are more vanadium vacancies and interstitial ions. The latter are surrounded by four vacancies as in the defect structure of Fe_xO. The oxygen ions around an interstitial vanadium ion are displaced away from it; oxygen and vanadium ions on the octahedrally coordinated sites exhibit strongly correlated displacements. There are anisotropic electron density distributions at vanadium ions near a vacancy. These effects indicate that the order–disorder transition is not due to a Jahn–Teller effect, but instead is a result of a long-range cooperative interaction, presumably due to the semimetallic nature of this oxide.

I. Introduction

VO_x contains large concentrations of cation and anion vacancies and interstitial vanadium ions (Watanabe, Andersson, Gjönnes & Terasaki, 1974; Morinaga & Cohen, 1976). An ordered structure has been detected in the composition range $VO_{1.2}$–$VO_{1.3}$ (Magnéli *et al.*, 1958; Westman & Nordmark, 1960; Westman, 1960; Andersson & Gjönnes, 1970; Bell & Lewis, 1971). As the oxygen sublattice is almost completely filled in this composition range, it has been suggested that the

* Now at Toyohashi University of Technology, Toyohashi, Aichi, 440, Japan.

0567-7394/79/050745-12$01.00

ordering involves cations and cation vacancies. The proposed models are summarized in Tables 1 and 2. It should be noted that the experimental techniques employed for the structure determination were rather minimal. The Andersson & Gjönnes model is illustrated in Fig. 1. With their limited data they were unable to show any shift of the ions from ideal sites. The proposed vacancy–interstitial cluster is based on that found in Fe_xO (Koch & Cohen, 1969), and on the extinctions in electron diffraction patterns, not on intensities. Some very weak additional reflections have been reported from this phase (Andersson & Gjönnes, 1970; Bell & Lewis, 1971). While there is some dispute whether these are due to multiple scattering and as to the range of compositions where they appear, Bell & Lewis modified the Andersson–Gjönnes model to give a unit-cell formula $V_{244}O_{320}$, in which some additional cation vacancies were added.

From qualitative studies of the diffuse intensity from the disordered phase, Andersson, Gjönnes & Taftö (1974) reported the nearest-neighbor intercluster vectors to be $a_c/2\langle 211\rangle$ and $a_c/2\langle 220\rangle$, whereas it is $a_c/2\langle 221\rangle$ in the ordered phase. This change seems unlikely. (The term a_c represents the lattice parameter of the cubic cell.)

The use of selected-area electron diffraction in several of these studies is dictated by the presence of a fine domain structure; it is difficult to analyze the many overlapping reflections by X-ray techniques. However, once the forbidden reflections have been established, by selected-area electron diffraction, more precise X-ray methods may be employed. This was the procedure

Table 1. *Proposed ordered structures*

Proposed model	Space group	Compositions	Authors
b.c.c. phases		$VO_{1.30}$ $VO_{1.20} \sim VO_{1.37}$ $VO_{1.20}$	Klemm & Grimm (1942) Gurevich & Ormont (1957) Magnéli *et al.* (1958)
$V_{204}O_{256}$*		$VO_{1.27}$	Westman & Nordmark (1960)
$V_{192}V_{256}$	$Ia3$ ($4 \times 4 \times 4$ disordered cells)	$VO_{1.28}$	Westman (1960)
$V_{52}O_{64}$	$I4_1/amd$	$VO_{1.23}$	Andersson & Gjönnes (1970)
$V_{244}O_{320}$	$I4_1/a$	$VO_{1.31}$	Bell & Lewis (1971)

* Unit-cell contents.

Table 2. *Comparison of the proposed ordered structures*

	Westman (1960)	Andersson & Gjönnes (1970)	Bell & Lewis (1971)
Unit cell	Actual composition $\sim V_{200}O_{256}$ with some vacant sites in $V_{192}O_{256}$ filled.	$V_{52}O_{64}$	$V_{244}O_{320}$
No. of tetrahedral vanadium ions	0	4	20
No. of octahedral vanadium vacancies	56	16	96
Configurations	Model *A* (two tetrahedral vacancy clusters sharing a corner, 8 per cell) Model *B* [hexagonal disc of vacancies on (111) and vacancy at center, 8 per cell]	Interstitial V + 4 surrounding vacancies isolated cluster, 4 per cell	Modification of the model by Andersson & Gjönnes
Technique	Weissenberg	Electron diffraction, powder patterns	Electron diffraction
R	≃39%	8% (14 powder peaks)	
Heat treatments and chemical composition	1073 K for 14 d ($VO_{1.27}$)	1063 K for 21 d, 1073 K for 5 d, or 873 K for 11 d ($VO_{1.2}$–$VO_{1.3}$)	973 K for 30 h, 973 K for 150 h, 853 K for 250 h ($VO_{1.25}$), 853 K for 150 h ($VO_{1.19}$)

employed here, to obtain more complete information on the ordered structure.

II. Experimental procedures

A. Specimen preparation

A large single crystal (diameter ~7 mm, length ~15 mm) of $VO_{1.30}$ was grown by the arc–Czochralski technique (Reed, 1967, 1969; Reed & Pollard, 1968). This crystal was grown in the tri-arc furnace at Lincoln Laboratories, under a flowing Ar gas atmosphere (purity 99·9%). A molybdenum stud was used instead of a seed crystal and the crystal growth rate was about 50 mm/h. This crystal was then wrapped in vanadium foil, and annealed at 1723 K for 1 d in an alumina tube under an argon atmosphere purified by passing it over heated Ti sponge. It was then slowly cooled by turning off the power of the furnace. The composition was determined with an accuracy of ±0·01 by measuring the weight change after combustion in air to the stoichiometric phase V_2O_5. The lattice parameter of this disordered phase was $a_c = 4{\cdot}1392\ (8)$ Å, which was determined with X-ray Debye–Scherrer patterns taken with filtered Cu $K\alpha$ radiation. This pattern did not indicate any V_2O_3; it was estimated ~9% could have been detected by comparing theoretical values of the strongest V_2O_3 powder line and the 200 reflection of VO_x and assuming that an intensity of 1% of the 200 intensity could have been detected. A cleaved specimen (~6 × 8 mm) was sealed in Vycor at $6{\cdot}5 \times 10^{-4}$ Pa and then held at 973 K for 30 h. This heat treatment followed that utilized by Bell & Lewis (1971); according to dark-field electron micrographs, small ordered domains (of diameter about 0·1 μm) are formed about equally on all three {100} habit planes of the original cubic structure (Andersson & Gjönnes, 1970; Bell & Lewis, 1971).

B. Extinctions

The X-ray diffraction patterns from such a specimen will then be overlapping patterns from three ordered domains on (100), (010) and (001) planes. Andersson & Gjönnes (1970) determined the forbidden conditions by selected-area electron diffraction:

Space group: $I4_1/amd$;
Unit cell: $a_1 = b_1 \simeq 2\sqrt{2}a_c, c_1 \simeq 2a_c$;
Extinctions:
hkl: $h + k + l = 2n$;
$hk0$: $h\ (k) = 2n$;
hhl $(l = 2n)$: $2h + l$ 2 4n.

In Fig. 2, the reciprocal axes of the proposed ordered phase, a_1^*, b_1^*, are given. The Bell & Lewis model, determined by electron diffraction, is also shown:

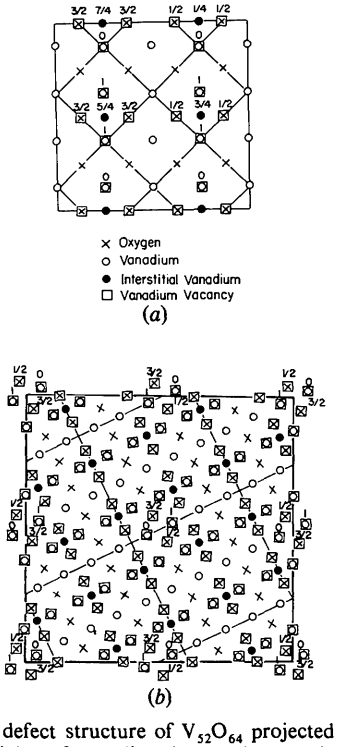

Fig. 1. (*a*) The defect structure of $V_{52}O_{64}$ projected on the (001) plane. The heights of vanadium ions and vacancies are in terms of the disordered unit-cell edge (Andersson & Gjönnes, 1970). For this ordered phase, $a = b \simeq 2\sqrt{2}a_c$, $c \simeq 2a_c$ where a_c is the dimension of the rock-salt-like disordered phase. (*b*) Bell & Lewis (1971) model.

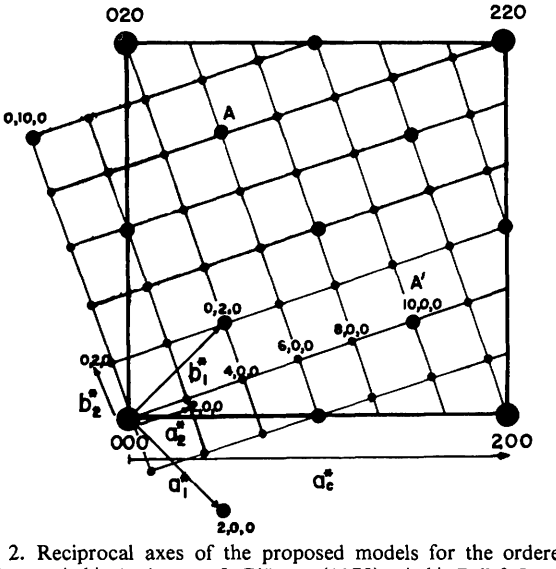

Fig. 2. Reciprocal axes of the proposed models for the ordered phase. a_1^*, b_1^*: Andersson & Gjönnes (1970); a_2^*, b_2^*: Bell & Lewis (1971); c_1^*, c_2^* axes are perpendicular to this plane. Largest spots, fundamental Bragg peaks; medium spots, superlattice peaks observed by Andersson & Gjönnes (1970); smallest spots, weak extra peaks observed by Bell & Lewis (1971).

Space group: $I4_1/a$;
Unit cell: $a_2 = b_2 \simeq 2\sqrt{10}a_c$, $c_2 \simeq 2a_c$;
Extinctions: $\begin{cases} hkl: h + k + l = 2n; \\ hk0: h\ (k) = 2n; \\ 00l: l = 4n. \end{cases}$

Also, the Westman model determined with X-ray Weissenberg photographs is represented in this figure:

Space group: $Ia3$;
Unit cell: $a_3 = b_3 \simeq c_3 \simeq 4a_c$;
Extinctions: $\begin{cases} hkl: h + k + l = 2n; \\ 0kl: k(l) = 2n. \end{cases}$

In Fig. 3(*a*), the positions of superlattice reflections in reciprocal space (following the Andersson & Gjönnes model) are shown schematically. The cell dimension along the *c* axis in the Westman model is $c \simeq 4a_c$, which is twice as long as that in the Andersson & Gjönnes model. (The 002 fundamental peak of the disordered phase is indexed as 008 in the Westman model, but 004 in the Andersson & Gjönnes model.) Thus, for the Westman model there are eight layers of superlattice reflections between the 000 and 002 fundamental peaks of the disordered phase, whereas for the Andersson & Gjönnes model (and also the Bell & Lewis model) there are four layers between them, as shown in Fig. 3(*a*). In the Westman model $l = 8n$ is one period in reciprocal space. (In Fig. 3*a*, the values, *l*, of Westman's indexing are also given.) Apparently, the odd-index layers of reflections ($l = 2n + 1$) in the Westman model are missing in the Andersson–Gjönnes model, and the locations of superlattice peaks in the even-index layers are also different in Fig. 3(*b*).

However, these discrepancies can be resolved by considering overlapping reflections from several ordered domains.

The co-existence of ⟨100⟩, ⟨010⟩ and ⟨001⟩ ordered domains implies that to consider the origin of the reflections from these domains we can interchange the coordinates of the reciprocal axes of the disordered phase, for example, $b^* \rightarrow c^*$. The reflections indicated by the symbols *P* in Fig. 3(*a*) in the plane *A* correspond to the reflections with the same symbols *P* in the ($l = 2n + 1$) layers in Fig. 3(*c*). A 90° rotation of reflections *P* around the b^* axis in Fig. 3(*a*) yields the reflections *P'* in Fig. 3(*c*). Similarly, for $l = 8n \pm 2$ layers, the appearance will be a combination of plane *B* (height $l = 2$) and plane *C*. Except for a few points (indicated by crosses in Fig. 3*c*), the pattern is coincident with that of Fig. 3(*b*), which is that reported by Westman (1960). The possible existence of these reflections indicated by crosses was examined in this study, but they could not be observed in the present experiments, although all other reflections in Fig. 3(*c*) were found. For instance, the pattern scanned along a ⟨100⟩ direction is shown in Fig. 4. There is a peak centered between the 200 and 400 reflections of the disordered phase but no peaks at $\frac{1}{4}$ and $\frac{3}{4}$ positions as would be expected following Westman (1960) (Fig. 3*b*).

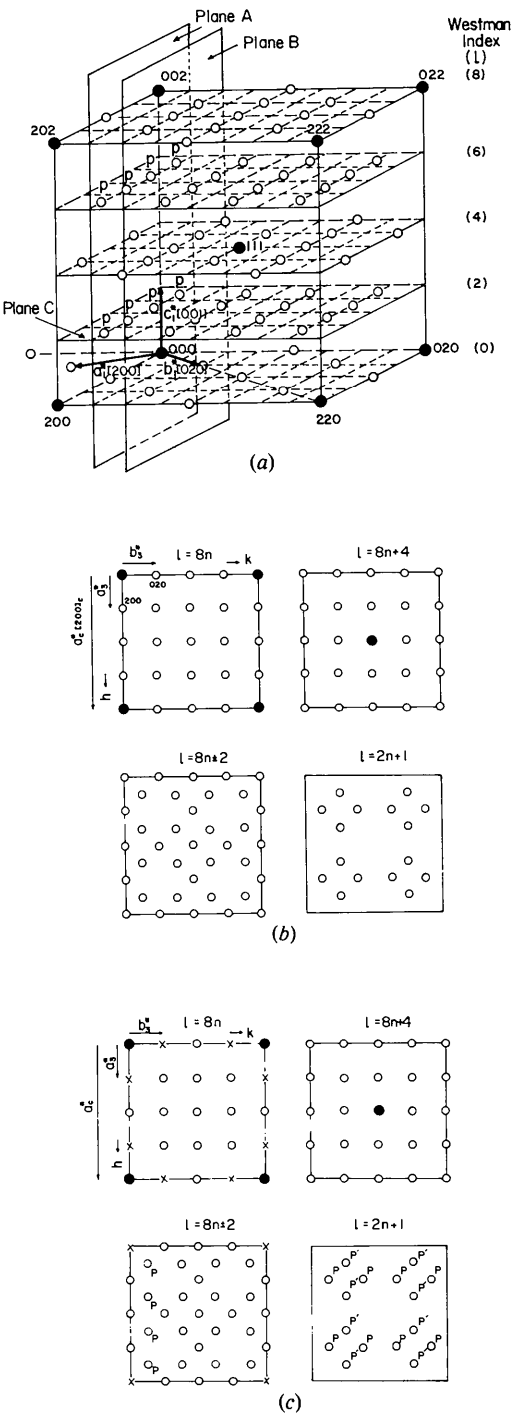

Fig. 3. (*a*) Superlattice spots (white circles) and fundamental reflections (black circles). The unit-cell axes chosen by Andersson & Gjönnes (1970) are shown. The indices are in terms of the cubic disordered phase. (*b*) Superlattice reflections (white circles) observed by Westman (1960), and fundamental spots (black circles). (*c*) Superlattice reflections expected from the extinction conditions of Andersson & Gjönnes (1970), assuming that there is overlapping of patterns from ordered domains with three ⟨100⟩ orientations; Westman's cell.

These results suggest that the ordered phase studied by Westman (1960) is the same as that studied by Andersson & Gjönnes (1970). The weakest extra spots in the electron diffraction pattern in Fig. 2 found by Bell & Lewis (1971) and Andersson & Gjönnes (1970), were not observed by Westman (1960), nor in the present experiments, even for long counting times (10 min at each point). At first it was thought that these peaks might be too weak to be observed with X-rays as the atomic scattering factors are much less than that for electrons. However, as shown in Fig. 5, such weak spots could not be found even in electron diffraction patterns. (These were taken from crushed pieces of a crystal with a 200 kV instrument.) All the superlattice peaks in these diffraction patterns can be explained by the reflections from the three domains, compare Fig. 5 with Fig. 3(*c*). Andersson & Gjönnes (1970) have reported that such weak spots appear only in the composition range of $VO_{1\cdot16}$ to $VO_{1\cdot20}$, but not in the range of $VO_{1\cdot20}$ to $VO_{1\cdot30}$, which agrees with the present result, but not with Bell & Lewis (1971). The change in composition probably induces additional modulations in the ordered structure.

Therefore, in the present experiment, X-ray intensities were obtained following the forbidden conditions reported by Andersson & Gjönnes (1970). No attempt was made to refine the cell parameters as the values of Westman (1960) and Andersson and Gjönnes (1970) yield interplanar spacings that differ in only the third decimal place.

C. X-ray measurements

Data were collected with a horizontal General Electric diffractometer equipped with a quarter circle eucentric goniometer, a scintillation detector, pulse height discriminator and controlled by a mini-computer (Richesson, Morrison, Cohen & Paavola, 1971). Mo $K\alpha$ radiation (wavelength $\lambda = 0{\cdot}71069$ Å, 50 kV, 18 mA), monochromatized by a pyrolitic graphite crystal bent to focus at the detector in the vertical direction, was employed. Filtered radiation was not suitable, because the background due to V fluorescence was too high to measure the weak intensities of superlattice reflections accurately. The pulse height analyzer was set for 90% acceptance of the Mo $K\alpha$. The receiving slit was opened until no increase in net intensity above background was observed for high-angle peaks (the slit opening was about 6 mm in width and 8 mm in height). The integrated intensities were measured by the normal θ–2θ step-scan technique in increments of 0·01° in 2θ, and repeated automatically until the statistical accuracy of the net intensity above background was less than 8%, a relatively high value, chosen because of the low intensities of the superlattice reflections. (The maximum intensity was about 500 Hz, but the intensity of most peaks was less than 100 Hz.) A flat slice of the crystal (with a face 6 × 8 mm) was used, which was larger than the incident beams at all angles.

The measured integrated intensities were corrected for the Lorentz–polarization factor and surface roughness. This correction for surface roughness was obtained by measuring the intensity of fluorescent V $K\alpha$ radiation near each reflection (de Wolff, 1956). Some 235 independent superstructure reflections were measured. Peak splitting due to a small tetragonality

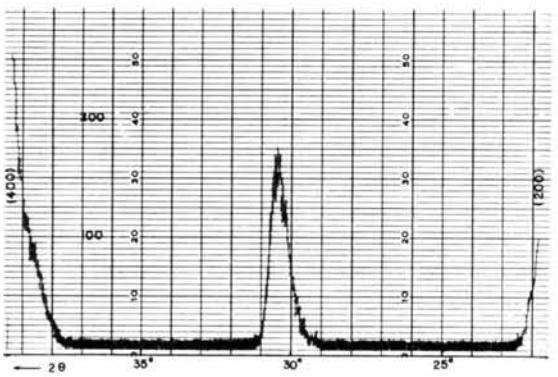

Fig. 4. X-ray pattern along |*h*00|. A superlattice peak exists between the 200 and the 400 Bragg reflections. (Experimental conditions: monochromatic Mo $K\alpha$, 50 kV, 18 mA.)

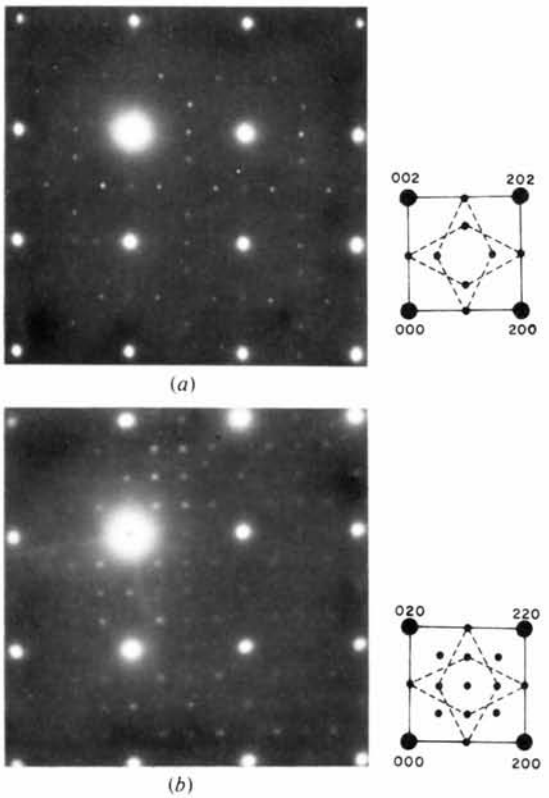

(*a*)

(*b*)

Fig. 5. Electron diffraction patterns from ordered $VO_{1\cdot30}$.

($c/a \simeq 0{\cdot}995$) and a domain structure could be distinguished readily from its position in reciprocal space, and measurements were carried out only for those peaks with satisfactory shapes.

III. Results

A. Qualitative features of the intensities of superlattice peaks

Along the [100] direction, the intensity distribution shows a sequence of 'strong' and 'weak' intensities with a period twice as big as the original f.c.c. reciprocal cell, Fig. 6(*a*). A similar sequence occurs along the [001] direction, Fig. 6(*b*), (*c*). If the ordered phase was due to ordering of the original disordered f.c.c. structure, the periodicity of the intensity should be equal to or less than the original f.c.c. reciprocal cell. For instance, in the case of vacancy ordering on the (100) and (200) planes of the f.c.c. unit cell with different numbers of vacancies on each plane, the periodicity of intensity is equal to the original f.c.c. reciprocal unit, although the superlattice peak appears in between two fundamental peaks (*e.g.* between 000 and 200 peaks) (Fig. 6*d*). This is not the intensity distribution found in Fig. 6(*a–c*).

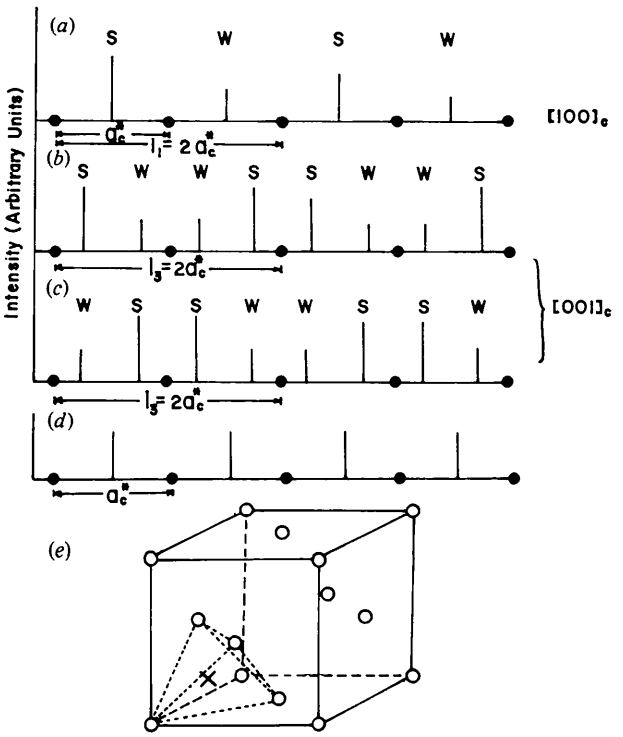

Fig. 6. Schematic intensity distribution of superlattice reflections along the [100] and [001] directions (*S*: strong, *W*: weak). a_c^* is the edge of the cubic reciprocal unit cell of the disordered structure. (*b*) and (*c*) occur for different *h*, *k*. In (*e*), a tetrahedral site in the disordered phase is indicated by a cross (×).

The most reasonable explanation for the observed intensity distributions is to introduce new lattice sites in the middle of the original disordered sites. As shown in Fig. 6(*e*), the likely sites are the tetrahedral interstitial sites of the close-packed oxygen sublattice. Thus, vanadium interstitials appear to be involved in the ordering.

B. The partial Patterson function

The partial Patterson function, $P\langle \mathbf{u,v,w} \rangle$, can be expressed in terms of the pair probability P_{AB}^{uvw} that the $\langle \mathbf{u,v,w} \rangle$ vector from an *A* atom terminates on a *B* atom (Koch & Cohen, 1969),

$$P\langle \mathbf{u,v,w} \rangle = N \left[(X_A Z_A + X_B Z_B)^2 + X_A X_B (Z_A - Z_B)^2 \times \left\langle 1 - \frac{P_{AB}^{uvw}}{X_B} \right\rangle \right]. \quad (1)$$

Here, N is the total number of atoms, Z_A and Z_B are atomic numbers, and X_A and X_B are atomic fractions. The first term on the right of (1) is the Patterson function of the average structure, which contributes to the intensity of fundamental reflections. The second term is the Patterson function of the extra peaks and represents deviations from a random array. Defining α^{uvw} by,

$$\alpha^{uvw} = 1 - \frac{P_{AB}^{uvw}}{X_B}, \quad (2)$$

this α^{uvw} is the well-known Warren short-range order parameter. Therefore, information on a derivative structure from the disordered state can be obtained when only the superlattice peaks are used in a Patterson synthesis (Frueh, 1953). From the partial Patterson map we may get the values of α^{uvw} by normalizing α^{uvw} with $\alpha^{000} = 1$ (Koch & Cohen, 1969). (Each α^{uvw} was actually obtained by taking the sum of heights $P\langle uvw \rangle$ in the region of a Patterson peak.)

According to (1) and (2), a positive peak in a partial Patterson map corresponds to $\alpha^{uvw} > 0$ and hence to $P_{AB}^{uvw} < X_B$; the number of *A–B* pairs connected by vector $\langle \mathbf{u,v,w} \rangle$ is lower than that for the case of a random solid solution. There is a preference for the atoms to choose like nearest-neighbors, which is commonly referred to as clustering. If *A* = vanadium ion and *B* = vanadium vacancy, a positive Patterson peak indicates that vanadium ions (or vacancies) have a tendency to gather together. On the other hand, a negative Patterson peak means that there is a preference for the atoms to choose unlike nearest-neighbors (short-range order). Thus a negative peak implies that vanadium ions pair with vacancies.

From the measured integrated intensities of the superlattice reflections, this partial Patterson synthesis

was obtained, assuming a tetragonal point group with Laue symmetry $4/mmm$ which satisfies the model of Andersson & Gjönnes. The results are given in Fig. 7. As the unit cell is the same as for the model of Andersson & Gjönnes, $u = 0{\cdot}5$ (or $v = 0{\cdot}5$) corresponds to the interatomic distance $\sqrt{2}a_c$ and $w = 0{\cdot}25$ corresponds to the distance $\frac{1}{2}a_c$.

In Fig. 7(*b*) negative peaks occur at $(\frac{1}{8}0\frac{1}{8})$ and $(0\frac{1}{8}\frac{1}{8})$ but not at $(\frac{1}{8}\frac{1}{8}0)$. These positions correspond to vectors between tetrahedral (interstitial) vanadium sites, and its first-neighbor octahedral vanadium sites. As indicated above, these negative peaks indicate that there are interstitial vanadium ions surrounded by vacancies at octahedral sites. Similar negative peaks were observed for Fe_xO (Koch & Cohen, 1969).

For comparison, the partial Patterson map made from the $V_{52}O_{64}$ model of Andersson & Gjönnes is given in Fig. 8. Figs. 7 and 8 are similar, but the heights of the negative or positive peaks are different. Following (1) and (2), α^{uvw} were calculated and the results are given in Table 3 (in which the values for Fe_xO are also listed for comparison). In Fe_xO, Koch & Cohen (1969) reported that there is a large vacancy cluster which consists of 4 interstitials and 13 surrounding vacancies. The larger positive values of α^{uvw} for first- and second-neighbor vectors for Fe_xO indicate the existence of a large vacancy cluster. However, for VO_x, α^{uvw} oscillates between positive and negative values for small interatomic vectors. This suggests that the ordered phase in VO_x is not made up of vacancy–interstitial clusters as large as in Fe_xO.

C. *Difference electron density maps*

The occupations of equipoints for the $V_{52}O_{64}$ model (Andersson & Gjönnes, 1970) are as follows:

Space group: $I4_1/amd$ (no. 141).

(1) 4 V in 4*a*,
(2) 16 V in 16*h*: $x = \frac{1}{8}, z = \frac{1}{4}$,
(3) 16 V in 16*f*: $x = \frac{1}{8}$,
(4) 16 V in 16*f*: $x = \frac{5}{8}$,
(6) 16 O in 16*h*: $x = \frac{1}{8}, z = 0$,
(7) 16 O in 16*h*: $x = \frac{1}{8}, z = \frac{1}{2}$,
(8) 32 O in 32*i*: $x = \frac{1}{8}, y = 0, z = \frac{1}{4}$.

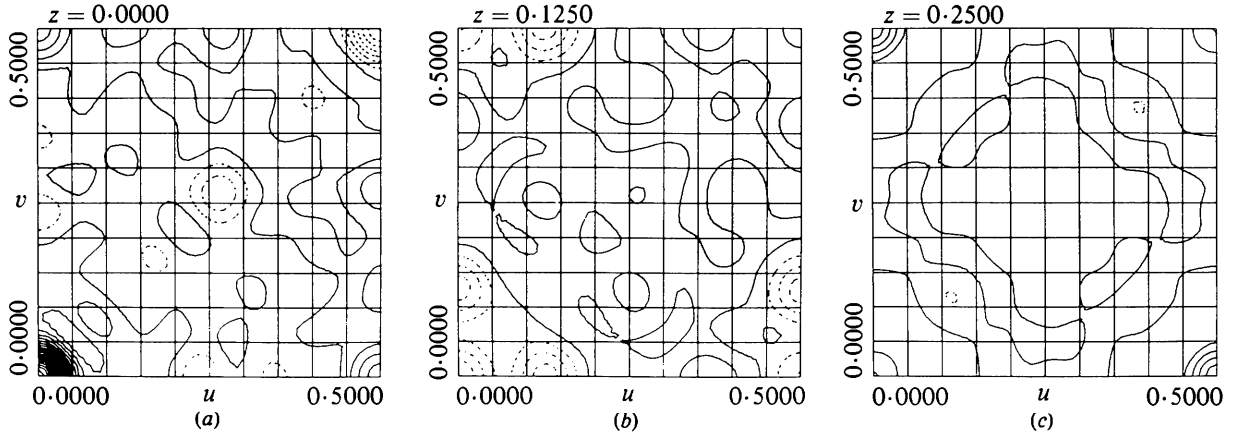

Fig. 7. Partial Patterson map from the observed superlattice peaks. [The height of Patterson peak at 0,0,0 is set to 999 and the interval of the contours is 50. For instance, the value of the negative peak (dotted lines) near $\frac{1}{3}$,0,$\frac{1}{8}$ is −187.]

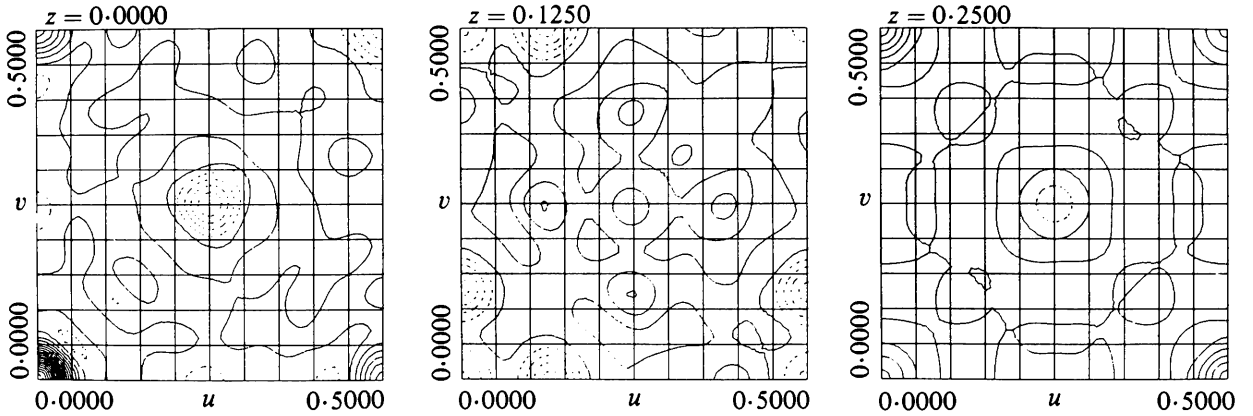

Fig. 8. Partial Patterson map from calculated intensities based on the model of Andersson & Gjönnes (1970). The height of the Patterson peak at 0,0,0 is set to 999, and the interval of the contours is 50.

Andersson & Gjönnes (1970) did not report values for the temperature factors of the ions, and claimed that displacements of ions were not helpful in reducing R. R was 23·4% with this model and our data, with unit weighting for each peak. To see what the difference is between the present experimental results and the original $V_{52}O_{64}$ model, a difference Fourier synthesis was performed. Large discrepancies appeared in the following three positions:

Table 3. *Comparison of short-range order parameters for the ordered phase and various models*

*i*th neighbour	4 × [*lmn*]*	Experimental	Andersson & Gjönnes model	After refinements	Fe_xO‡
Type 1 vectors†					
–	000	1·000	1·000	1·000	1·00
1	220	−0·083	−0·038	−0·085	0·57
	202	0	0	0	
2	400	−0·125	−0·212	−0·109	0·35
	004	−0·407	−0·293	−0·452	
3	422	0	0	0	0·00
	224	0·055	0	0·021	
4	440	0·153	0·240	0·173	0·06
	404	−0·125	−0·212	−0·112	
	620	0·055	0	0·019	
5	602	0	0	0	0·11
	206	0	0	0	
6	444	0·153	0·240	0·188	−0·21
	642	0	0	0	
7	624	−0·083	−0·041	−0·085	−0·26
	426	0	0	0	
Type 2 vectors†					
	200	0	−0·010	0	
	002	0·055	0·074	0·049	
	222	0	0	0	
	420	0	0	0	
	402	0	−0·044	0	
	204	0	0	0	
	600	0	0	0	
	006	0·055	0·074	0·049	
	442	0·176	0·151	0·159	
	424	0	0	0	
	622	0	0	0	
	226	0	0	0	
Type 3 vectors†					
	111	−0·187	−0·195	−0·166	
	311	0·048	0·073	0·037	
	113	0·074	0·046	0·072	
	331	0·084	0·041	0·091	
	133	0	0·026	0	
	333	−0·179	−0·201	−0·178	
	511	0	0·026	0	
	115	0·074	0·046	0·072	

* [*lmn*] are indexed based on the axes of the cubic disordered phase.

† Type 1 vectors *l*,*m*,*n* all [2*p*]/4, $l + m + n = [4q]/4$.
Type 2 vectors *l*,*m*,*n* all [2*p*]/4, $l + m + n = [4q + 2]/4$.
Type 3 vectors *l*,*m*,*n* all [2*p* + 1]/4.

‡ For Fe_xO, the analysis was carried out with cubic symmetry, so for instance $\frac{1}{2}\frac{1}{2}0$ and $\frac{1}{2}0\frac{1}{2}$ can be taken as the same vectors, but for VO_x with tetragonal symmetry, these are distinct vectors.

(1) 16*h* (*e.g.* at $\frac{3}{8}\frac{1}{4}0$): large positive peak;
(2) 16*f* ($x = \frac{5}{8}$) (*e.g.* at $\frac{5}{8}00$): large negative peak;
(3) 16*g* ($x = \frac{1}{4}$) (*e.g.* at $\frac{1}{4}0\frac{1}{8}$): large positive peak,

where 16*g* is an interstitial position which is not included in the original $V_{52}O_{64}$ model. As the 16*h* positions are already fully occupied by vanadium ions, and the positive peak is surrounded by negative contours, this peak is probably due to incorrect temperature factors. The other two peaks are *not* surrounded by contours of opposite sign. Therefore, these results suggest that (i) there are vacancies in the 16*f* positions, (ii) there are interstitials in the 16*g* positions. Least-squares refinements on $|F|$ were carried out (Busing, Martin & Levy, 1960, as modified by Ibers) with respect to (*a*) the concentration (multiplier) for each equipoint, (*b*) displacements of oxygen and vanadium ions, and (*c*) isotropic temperature factors for individual sites. (Allowing for anisotropic temperature factors did not improve the analysis substantially.) The final R was 17·8% with unit weighting for each peak and 19·5% with weighting inversely proportional to the net intensity. The expected R according to Hamilton (1965) [with $\alpha = \frac{1}{2}\sigma(F^2_{obs})/F^2_{obs}$] is 4%. (Calculated and observed structure factors are available in Morinaga, 1978.) The results are given in Table 4. (Only the results for variation of the 16*f* and 16*g* equipoints are shown; the others were tried without any noticeable effect on R.) The short-range order parameters were calculated and the results are given in Table 3. A difference Fourier map still revealed a large peak at $x = 0{\cdot}1$, $y = 0{\cdot}25$ and $z = 0$, which is close to the position of the vanadium vacancies, and this will be discussed below.

D. The possibility of space groups other than $I4_1/amd$

To proceed to a smaller R, the number of adjustable parameters could be increased, which suggests a space group with lower symmetry than $I4_1/amd$. However, for space groups with tetragonal symmetry, only $I4_1/amd$ can explain the extinctions.

One trial was carried out with space group $Fdd2$ (No. 43) and one with $I4_1/amd$ (No. 80).

These space groups were chosen with the following in mind:

(1) The atomic occupations should follow those of the $I4_1/amd$ space group, but the existence of local strains could reduce the symmetry.

(2) The partial occupation of equipoints may cause ambiguities in selecting a space group; there could be weak peaks that were not detected (although electron diffraction patterns were examined).

(3) The observed pattern includes overlapping effects of reflections coming from ordered domains with either [001] or [00$\bar{1}$] type orientations. (The overlapping from other orientations of domains was eliminated as described earlier.)

The unweighted R index dropped to 15·6% for the $Fdd2$ space group and to 14·8% for $I4_1$ after refinements with respect to (*a*) concentration (multiplier), (*b*) displacements and (*c*) isotropic temperature factors for individual sites. The occupation of ions was basically that for the model in the previous section. However, superlattice reflections which were not observed in the experiments appear in the calculations, some as intense as the observed peaks, for instance, for the space group $I4_1$, the 114, 334 and 554 reflections. The selection of space group $I4_1/amd$, appears the most reasonable.

IV. Discussion

The refinements of the $V_{52}O_{64}$ model originally proposed by Andersson & Gjönnes (1970) carried out in this study indicate some significant deviations.

(*a*) There are vacancies at the 16*f* positions.

(*b*) There are interstitial vanadiums at 16*g* near these vacancies.

The overall composition is similar to that of a spinel (*e.g.* $Fe_3O_4 = FeO_{1.3}$) and such a structure involves interstitial–vacancy tetrahedral clusters as found in this ordered phase, but its interstitial concentration is 12·5%, much larger than that of the present structure (~3%). The composition from the X-ray results is $VO_{1.24}$, but the overall composition is $VO_{1.30}$. This cannot be due to V_2O_3 as ~20% would be required and 9% could have been detected in the powder patterns we examined, assuming the level of detection was 1% of the intensity of the strongest peak from VO_x (see *Specimen preparation*). Perhaps there is a mixture of domains, ordered $VO_{1.24}$ and V_2O_3, suspended in a disordered matrix of $VO_{1.30}$. Volume fractions from electron microscopy could corroborate such suggestions. Anyway, small changes in the composition would not alter R appreciably.

There are three interesting observations concerning the atomic displacements that we will discuss in turn.

A. Displacements of oxygen ions near interstitial vanadium ions

In Fig. 9, a model of the ordered phase is shown in four layers with heights $z = 0$, $\frac{2}{8}$, $\frac{4}{8}$, and $\frac{6}{8}$. (The periodicity in the z direction is $2a_c$.) The interstitial vanadium ions are on the layers $z = \frac{1}{8}$, $\frac{3}{8}$, $\frac{5}{8}$ and $\frac{7}{8}$, and their positions are given in the $z = 0$, $\frac{2}{8}$, $\frac{4}{8}$, and $\frac{6}{8}$ layers by indicating the height z in parentheses. The number given near each ion corresponds to the site numbers in Table 4. The directions of displacements are indicated by arrows. Positive and negative signs imply that there is a component of the displacements in the positive or negative z direction, as well as in the direction shown.

The interstitial vanadium ion is surrounded by oxygen ions in the No. 6 equipoint. In Fig. 10 the displacements of oxygen ions around such a vanadium ion are examined. These oxygens are displaced in directions away from this interstitial. This displacement mode is close to the A_1 mode for an XY_4-type molecule, Fig. 11 (Murrell, Kettle & Tedder, 1965).

In 3*d* transition-metal compounds it is well known that the anisotropy of *d* orbitals is distorted. For instance, there is a general theorem due to Jahn and Teller (*e.g.* see Englman, 1972), which states that if a

Table 4. *The refined structure of the ordered phase (space group $I4_1/amd$) and a comparison with the model of Andersson & Gjönnes* (1970)

		Andersson & Gjönnes model*		Refined structure		
Site number	Sites	Number of ions	Positions	Number of ions	Positions	B (Å^2)
(1)	4*a* (Interstitial sites)	4 Vanadiums		4 Vanadiums		1·41 (15)
(2)	16*h*	16 Vanadiums	$x = 0·125$ $z = 0·250$	16 Vanadiums	$x = 0·12380$ (49) $z = 0·25050$ (50)	0·75 (07)
(3)	16*f*	16 Vanadiums	$x = 0·125$	16 Vanadiums	$x = 0·12520$ (51)	1·24 (08)
(4)	16*f*	16 Vanadiums	$x = 0·625$	14·95 (33) Vanadiums	$x = 0·62250$ (51)	1·06 (09)
(5)	16*g* (Interstitial sites)	0 Vanadiums		0·66 (18) Vanadiums	$x = 0·250$	0·75 (55)
(6)	16*h*	16 Oxygens	$x = 0·125$ $z = 0·000$	16 Oxygens	$x = 0·11820$ (218) $z = 0·00920$ (214)	1·55 (60)
(7)	16*h*	16 Oxygens	$x = 0·125$ $z = 0·500$	16 Oxygens	$x = 0·12910$ (218) $z = 0·49730$ (214)	1·18 (51)
(8)	32*i*	32 Oxygens	$x = 0·125$ $y = 0·000$ $z = 0·250$	32 Oxygens	$x = 0·12980$ (168) $y = 0·00330$ (171) $z = 0·25060$ (119)	1·05 (49)

* This model of Andersson & Gjönnes (1970) was not refined with respect to the displacements of ions.

non-linear molecule is in an orbitally-degenerate energy level, the system will distort so as to relieve this degeneracy, and since electrons occupy the lower energy levels there are attendant energy gains due to this distortion. The strain energy increases with distortions and a balance between the electronic and elastic energy determines the actual magnitude of distortion in any material. Since the ordered phase is made up of $[VO_4]$ 'molecules', the distortion of oxygen ions in this molecule may be important. If the t_{2g} orbitals in cubic fields are partially filled (but *not* half full), a tetragonal distortion may be expected due to the anisotropy of the *d* orbitals, as in Fig. 11(*b*) (Goodenough, 1966). The displacements of oxygen ions in such a case are like the *E* mode in Fig. 11(*a*), but the observed displacements are close to the A_1 mode. The charge at the interstitial vanadium ion in the ordered phase is unknown. If it is $V^{2+}(d^3)$, Goodenough's discussion is not applicable as the t_{2g} orbital is only half filled, but there is evidence for a lower valency in this system (Watanabe *et al.*, 1974; Morinaga & Cohen, 1976). Also, there is no evidence that at the interstitial vanadium ion the t_{2g} energy level is lower than the e_g energy level. However, in spite of this uncertainty it is clear that the observed A_1 mode cannot be explained by anisotropy of the *d* orbitals. The displacements of oxygen ions near an interstitial vanadium ion do not represent what is expected due to electron orbital anisotropy with the observed tetragonality ($c/a < 1$). The local *d* electron configuration does not appear to play a role in the displacements of ions; the elastic or electrostatic energy seems to be more important.

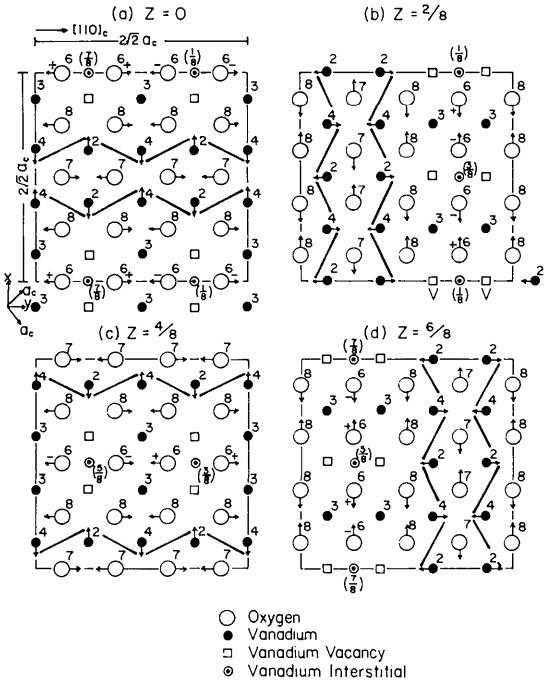

Fig. 9. The displacements of vanadium and oxygen ions. The numbers in parentheses indicate the level. The other numbers refer to the site numbers in Table 4. Signs indicate direction of *z* component of displacement.

B. Displacements of vanadium and oxygen ions at octahedral sites

As can be clearly seen in Table 4, the displacements of ions along the *z* direction from ideal positions are not large except for the No. 6 oxygen ions, which were discussed above. But, there are significant *x* displacements (except for the No. 3 vanadium ions). In Fig. 9, the directions of displacements for ions which are larger than the experimental error (two times the standard deviations), are indicated by arrows. Consider the ions on the $z = \frac{2}{8}$ layers:

(*a*) The No. 2 vanadium ions which are near a vacancy (*V*), approach the vacancy.

(*b*) The No. 8 oxygen ions move away from vacancy pairs (*V*–*V*): this direction might have been expected due to the electrostatic interaction between the No. 8 oxygen ions (negative charge) and the vacancies

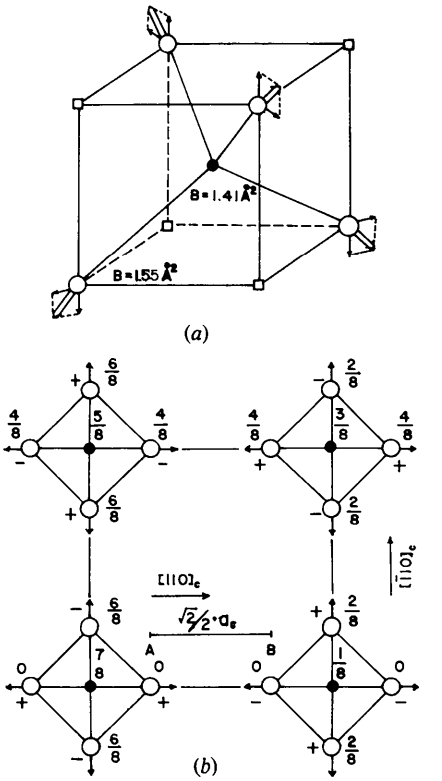

Fig. 10. (*a*) Displacements of oxygen ions near an interstitial vanadium; the oxygen ions are in the (6) 16*h* positions: $x = 0{\cdot}1182$ (22), $z = 0{\cdot}0092$ (21); ideal positions: $x = 0{\cdot}1250$, $z = 0{\cdot}000$, displacements: $\Delta x = -0{\cdot}007$, $\Delta z = +0{\cdot}009$. (*b*) The arrangements of $[VO_4]$ 'molecules' in the ordered phase. (The number on each ion indicates the *z* coordinate.)

(negative effective charge). The approach of the No. 2 vanadium ions to neighboring vacancies is probably due to attractive electrostatic interaction.

(*c*) The No. 7 oxygen ions approach neighboring No. 2 vanadium ion pairs.

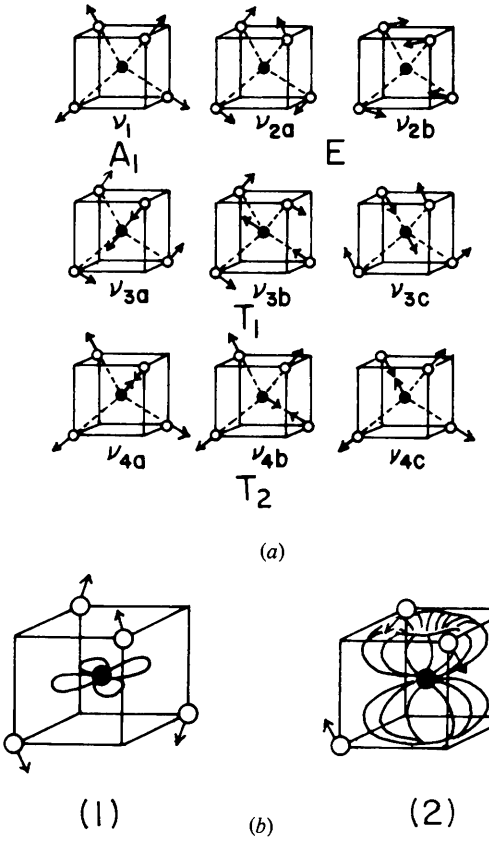

Fig. 11. (*a*) Nine normal displacement (or vibrational) modes of an XY_4 type molecule. Adapted from Murrell *et al.* (1965). (*b*) The tetragonality induced by the anisotropy of *d* orbitals, (1) d_{xy} orbitals and (2) $(d_{yz} + id_{zx})$ orbitals. Adapted from Goodenough (1966).

(*d*) The No. 4 vanadium ions displace toward the neighboring No. 7 oxygen ions. The results (Fig. 9*c* and *d*) may be due to either electrostatic or elastic relaxation.

(*e*) The No. 3 vanadium ions do not show appreciable displacements. This is probably due to the fact that most of the No. 3 vanadium ions are neighbors to two symmetrically located vanadium vacancies. The oxygen ions, No. 6 and No. 8, surrounding the No. 3 vanadium ion displace symmetrically with respect to the No. 3 vanadium site.

As a result of these correlated displacements, the vanadium ions (and oxygen ions) form a wave-like chain along the $[110]_c$ direction on each (001) layer. For example, the displacements of the No. 2 and No. 4 vanadium ions are indicated in Fig. 9 with heavy lines. When the oxygen tetrahedron shrinks, the vanadium tetrahedron expands, and *vice versa*. These correlated displacements cannot be explained by local *d*-electron configurations at vanadium sites; long-range correlative forces must be important.

C. Anisotropic electron density of vanadium ions near vanadium vacancies

Because of the displacements it is interesting to examine the anisotropy of the electron density at vanadium or oxygen sites near a vacancy. Difference electron density maps are given in Fig. 12. A spherical electron density has been assumed, since isotropic temperature factors were used for the individual ions and also the atomic scattering factors employed do not involve any anisotropic effects. Therefore, if the difference electron density maps show lobes, this would be an indication of the existence of anisotropic electron density distributions (which may be either dynamical or static).

The notations in Fig. 12 follow those in Table 4; for instance, '2V' implies the vanadium ion at the 16*h* position. A large *V* means a vacancy, and (*I*) means

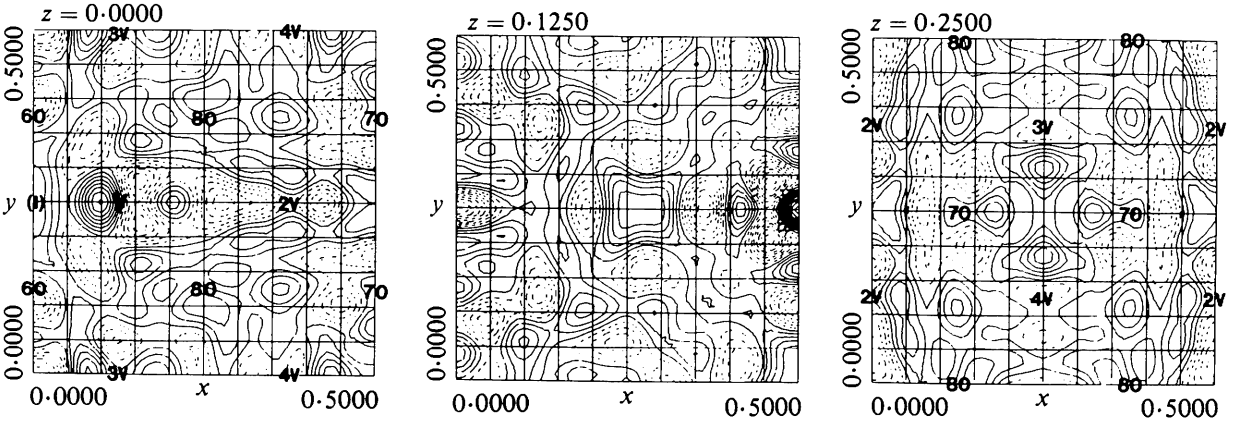

Fig. 12. Difference electron density map made with the observed intensities minus the calculated ones after refinements.

that there is an interstitial vanadium ion which is not on the $z = 0{\cdot}0$ plane but on the $z = -\frac{1}{8}$ plane (refer to Fig. 9). The contour interval is about 0·3 e $Å^{-3}$. The positive peak at $x = 0{\cdot}1$ and $y = 0{\cdot}25$ is about 2·1 e $Å^{-3}$ and broken (negative) contours begin at −0·3 e $Å^{-3}$.

Referring to Fig. 12:

(1) The oxygen ions (No. 6, No. 7 and No. 8) are approximately spherical.

(2) The vanadium ion No. 4 appears nearly spherical but the vanadium ions No. 2 and No. 3, which are neighbors to a vacancy, show lobes indicating that there are anisotropic electron distributions on these sites.

(3) At the vanadium vacancy site (V), there are distorted contours indicating that there may be some effective electron density at this location.

As will be shown in Part II, in the disordered phase there is a large size effect scattering due to local lattice distortions. The short-range order parameters obtained after correcting for this size effect scattering are similar to those of the ordered phase, obtained here from a partial Patterson synthesis. This indicates that the large distortions in the disordered phase are reduced in the ordered phase, presumably because of the periodic arrangements of vacancies.

This research was sponsored by the US Army Research Office under Grant No. DAAG-29-78-G-0156. Portions of the work were carried out in the long term X-ray facility of Northwestern University's Materials Research Center, supported in part by NSF through grant No. DMR-76-80847. We especially thank Dr T. Reed and Mr R. Fahey for their help during our stay at Lincoln Laboratories to grow crystals.

This study constituted a portion of the thesis (by MM) submitted in partial fulfilment of the requirements for the PhD degree at Northwestern University.

References

ANDERSSON, B. & GJÖNNES, J. (1970). *Acta Chem. Scand.* **24**, 2250–2252.

ANDERSSON, B., GJÖNNES, J. & TAFTÖ, J. (1974). *Acta Cryst.* A**30**, 216–224.

BELL, P. S. & LEWIS, M. H. (1971). *Phys. Status Solidi*, **7**, 431–439.

BUSING, W. R., MARTIN, K. O. & LEVY, H. A. (1960). *ORFLS*. Report ORNL-TM-305. Oak Ridge National Laboratory, Oak Ridge, Tennessee.

ENGLMAN, R. (1972). *The Jahn–Teller Effect in Molecules and Crystals*. New York: Wiley–Interscience.

FRUEH, A. J. (1953). *Acta Cryst.* **6**, 454–456.

GOODENOUGH, J. B. (1966). *Magnetism and the Chemical Bond*. New York: Interscience.

GUREVICH, M. A. & ORMONT, B. F. (1957). *Zh. Neorg. Khim.* **2**, 2581–2588.

HAMILTON, W. C. (1965). *Proceedings of the Symposium on Accuracy in X-ray Intensity Measurement*, pp. 12–32. New York: The American Crystallographic Association.

KLEMM, W. & GRIMM, L. (1942). *Z. Anorg. Allgem. Chem.* **250**, 42–55.

KOCH, F. & COHEN, J. B. (1969). *Acta Cryst.* B**25**, 275–287.

MAGNÉLI, A., ANDERSSON, S., ÅSBRINK, S., WESTMAN, S. & HOLMBERG, B. (1958). Final Tech. Rep. No. 1, US Dept. of Army, DA091-508-EUC-245.

MORINAGA, M. (1978). PhD Thesis. Northwestern Univ., Evanston, Illinois.

MORINAGA, M. & COHEN, J. B. (1976). *Acta Cryst.* A**32**, 387–395.

MURRELL, J. N., KETTLE, S. F. & TEDDER, J. M. (1965). *Valence Theory*. New York: John Wiley & Sons.

REED, T. B. (1967). *Mater. Res. Bull.* **2**, 349–367.

REED, T. B. (1969). Proc. Third Int. Symposium of High Temperature Technology, Asilomar, California, pp. 655–664.

REED, T. B. & POLLARD, E. R. (1968). *J. Cryst. Growth*, **2**, 243–247.

RICHESSON, M., MORRISON, L., COHEN, J. B. & PAAVOLA, K. (1971). *J. Appl. Cryst.* **4**, 524–527.

WATANABE, D., ANDERSSON, B., GJÖNNES, J. & TERASAKI, O. (1974). *Acta Cryst.* A**30**, 772–776.

WESTMAN, S. (1960). Final Tech. Rep. No. 1, US Dept. of Army, DA-91-591-EUC-1319.

WESTMAN, S. & NORDMARK, C. (1960). *Acta Chem. Scand.* **14**, 465–470.

WOLFE, P. M. DE (1956). *Acta Cryst.* **9**, 682–683.